Nigerian Journal of Physics (NJP)
ISSN online: 3027-0936
ISSN print: 1595-0611
DOI: https://doi.org/10.62292/njp.v35i2.2026.515
Volume 35(2), June 2026

Mapping and Depth Estimation of Magnetic Sources of the Chad Basin, Nigeria Using High Resolution Aeromagnetic Data

*[1]Kehinde S. Ishola, [2]Olawale B. Olatinsu, [1]Christopher E. Okagu and [1]Olumide Omojola

[1]Department of Geosciences, University of Lagos, Akoka, Lagos, Nigeria.
[2]Department of Physics, University of Lagos, Akoka, Lagos, Nigeria.

*Corresponding author: kishola@unilag.edu.ng Phone: +2348133727590

ABSTRACT

The Chad Basin is an intracontinental basin originated from the actions of a number of peripheral uplifts making a periodic study of this basin imperative. On this background, an aeromagnetic data of the Chad Basin was used to identify some magnetic anomalies and determine the depth of the magnetic sources. The residual map obtained from the application of first order polynomial fitting to the total magnetic intensity data, revealed two magnetic anomalies. The low frequency anomalies emanated from the deep seated bodies with thicker sediments and perceived to be the magnetic basement while the high frequency anomalies resulted from shallower geologic bodies regarded as the sediments cover. The lineaments map showed that the long regional trends that lie in the directions ENE–WSW, WNW–ESE and E–W control the subsurface structure beneath the studied area. The magnetic field amplitudes vary from a maximum of 223 nT to a minimum of 96 nT depicting varying magnetic highs and lows as possible indication of undulating basement surface and magnetic traps. The depth to the basement range from about 0.5 km in the south to 3.0 km and deepens towards the north. The energy power spectrum estimated an average depth to the top of regional sources is about 7 km while the shallow sources have an average depth of about 1.5 km to their magnetic sources.

Keywords:
Aeromagnetic,
Magnetic Anomalies,
Lineament,
Depth to Source,
Power Spectrum.

INTRODUCTION

In the last five decades, a very large number of both ground and airborne geophysical techniques have been developed and executed to assist in subsurface structural mapping for environmental, mineral/hydrocarbon and groundwater purposes (Feder, 1962; Lattman, 1963; Rydstrom, 1967; Hood and Ward, 1969; Smith et al., 2004; Meng et al., 2006; Cox et al., 2012; Auken et al., 2017; Noh et al., 2020; Biswas and Sharma, 2020; Liang et al., 2021). Ground and airborne magnetic surveys are used at just about every conceivable scale and for a wide range of purposes such as detailed mapping of some geological features e.g., faults, shear zones, folds, alteration zones and other structures (Olson, 1970; Nabighian, 1972, 1974, 1984; Kearey et al., 2002; Sharma, 2002; Rajaram, 2009; Nabighian et al., 2005; Raimi et al., 2014). The use of ground geophysical techniques are usually more effective when used to explore targets already identified by the airborne methods in an integrative approach. In this regard, airborne methods are usually the most cost-effective tools available for both large regional reconnaissance surveys and employed as aids not only in geological mapping but also in locating target areas for a more detailed follow-up (Palacky, 1981; Reeves, 2005; Christensen et al., 2015).

Airborne magnetic in particular can detects the subtle variations in the earth's magnetic field arising from the presence or absence of ferromagnetic minerals such as magnetite (Fe_3O_4), maghemite (Fe_2O_3), pyrrhotite (FeS) and ilmenite (FeTiO_3) (Styles, 2012). These minerals are commonly associated with stream-bed deposits and are often associated with subsurface drainage paths (paleochannels) that may serve as conduits for groundwater flow (Srivastava, 2002; Joel et al., 2016; Djamel, 2017; Okpoli and Akinbulejo, 2022). Furthermore, these minerals are common in many igneous rocks, both as primary and secondary minerals, and can often be used to depict and delineate geological structures (e.g. faults, dykes) in the subsurface from discontinuities seen in the airborne images (Rambabu

and Sinha, 1986; Kivior and Boyd, 1998; Osinowo et al., 2013; Akinlalu et al., 2018).

Furthermore, aeromagnetic surveys have continued to aid in the discovery of hydrocarbon reservoirs, radioactive elements such as uranium, titanium, base and precious metals (Reford and Butt (1983); Genik (1992); Elliott and Laharia (2008); Innocent et al. (2008); Ogah and Abubakar (2024)). This can effectively be carried out if the resolution of the aeromagnetic data which depends upon the distance between the traverse line spacing, the distance between the aircraft and the ground, the magnetic signature of the aircraft itself, and variations in the diurnal activity is given priority among other factors (Reeves, 2005).

The subsurface geology of the Chad Basin requires periodic investigations to be carried out with a view to updating our better our understanding of the dynamics of the basin. However, considering the state of insecurity especially in the northeastern Nigeria, the acquisitions of land geophysical data has been hampered by the nefarious activities of some groups or sects thus making the use of airborne magnetic technique as an alternative mode of data gathering in the area of study. Hence, this study was aimed at the identification of some magnetic anomalies of the observed aeromagnetic data of Chad Basin in order to achieve the following objectives (i) map the orientations of structural features within the Basin (ii) delineate the basin geometry or configuration (iii) determine the depth to magnetic basement sources.

Description and Geology of the Study Location

The study area is bounded by Latitudes 12° 00' – 13° 00' N and Longitudes 13° 00' – 14° 00' E in Northeastern Nigeria (Figure 1) with an area of approximately 27,500 square kilometers. It is so large that it covers about nine Local Government Areas which are Mafa, Konduga, Jere, Dikwa, Gazamala, Kukawa, Marte, Monguno, and Nganzai as shown in Figure 2. The Bornu Basin is a Nigerian sector of the Chad Basin representing about one-tenth of the total area extent of the Chad Basin. The Chad Basin belongs to the African Phanerozoic sedimentary basins whose origin is related to the dynamic process of plate divergence. Notable exceptions, however, are the deformed basinal sequences of the Paleozoic fold belts of Morocco and Mauritania which resulted from the Hercynian convergent motion and collision of Africa and North America, and the Tindouf and Ougarta basins which are Paleozoic successor basins (Burke, 1976; Petters, 1982). It is an intracratonic inland basin covering a total area of about 2,335,000-kilometer square with Niger and Chad Republics sharing more than half of the basin. The basin belongs to a series of Cretaceous and later rift basins in Central and West Africa whose origin is related to the opening of the South Atlantic (Obaje et al., 2004). Geographical evidence suggests that the Cretaceous rocks occupy broad troughs in the Basement Complex (Cratchley et al., 1984). The Kerri-Kerri Formation which composed of basal conglomerate, grit, sandstone, siltstone and clay sediments is formed during the Paleocene age. These sediments are unfolded and are warped gently to the north-east beneath the Chad Formation. The youngest deposits are the river alluvium and deltaic and lagoon clay flats which blanket wide areas to the south and south-west of Chad (Grove and Pullan (2017); Carter et al. (1963)).

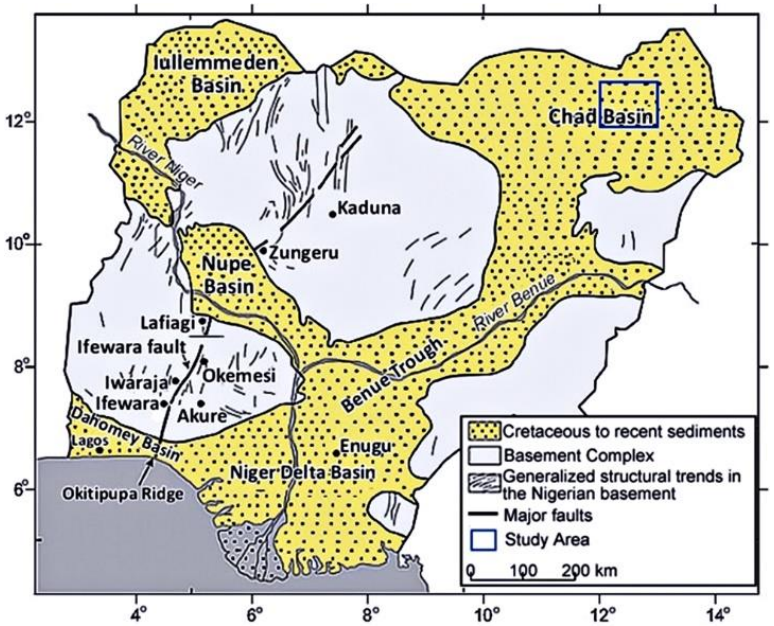

Figure 1: Map of Nigeria Showing Bornu-Chad Basin (Obaje (2009); Arogundade et al.(2020))

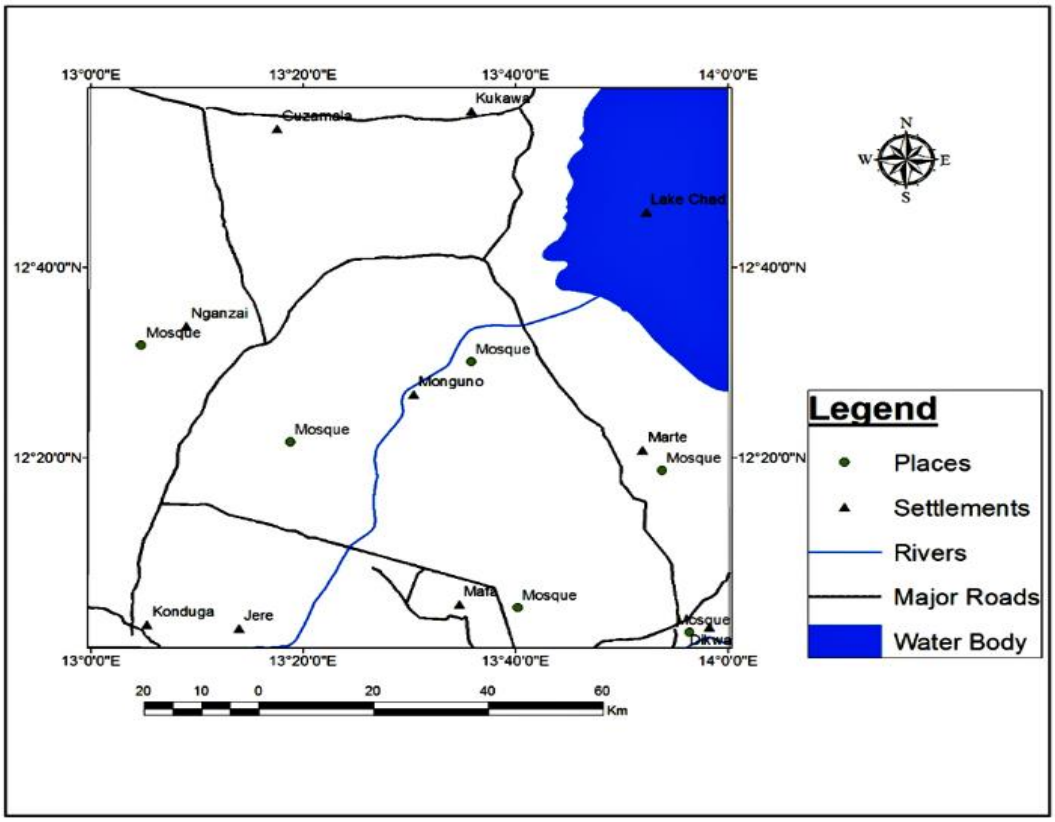

Figure 2: Map of the Study Area, Showing the Various Local Government Areas

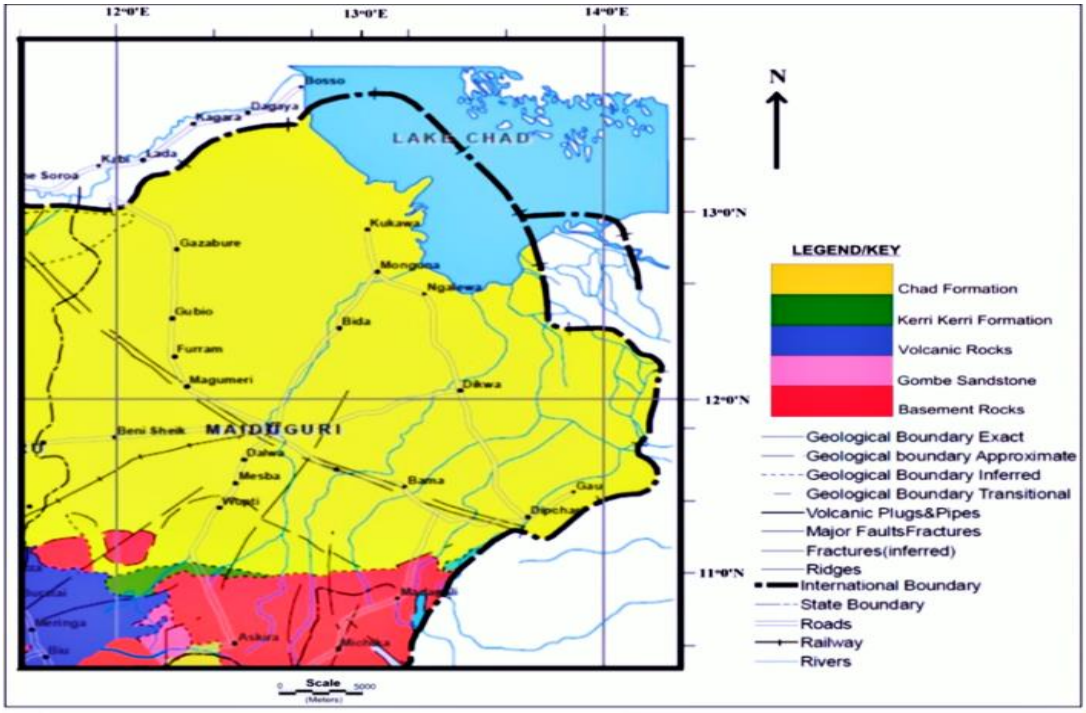

Figure 3: Geologic Map of the Chad basin. Source: Geological and Mineral Resources Map, Nigerian Geological Survey Agency (NGSA, 2006)

MATERIALS AND METHODS

Data Collection

Aeromagnetic data of the Chad basin was obtained from the National Geological Survey Agency, Nigeria. The data consists of profiles or flight lines plotted on continuous strip chart. The aeromagnetic data was collected at a nominal flight altitude of 152.4 m along north–south flight lines (nearly perpendicular to predicted geological strikes), spaced approximately 2 km apart and the component of the magnetic field measured was the total magnetic field intensity. The study area covered eleven aeromagnetic sheets with sheets numbers: 202, 203, 204, 205, 206, 207, 208, 225, 226, 227 and 228. The magnetic data were digitized as text file of the form (X, Y, Z) with X and Y representing the Longitude and Latitude of the study area in Universal Transverse Mercator (UTM) in meters respectively while the Z represents the Total Magnetic field Intensity (TMI) measured in NanoTesla (nT) and then merged. The combined data sets were pre-processed, analysed and interpreted both qualitatively and quantitatively. Qualitative interpretation of the field data was carried out by visual inspection of the total magnetic intensity (TMI) map. The quantitative interpretation which involved all numerical analytical functions applied on the potential field data was considered a backbone for all the interpretation methods. The initial stages of quantitative magnetic data interpretation involved the application of mathematical filters to the observed data. The purpose of filtering was to enhance magnetic anomalies of interest and to gain some basic information on source locations. The upward continuation operation smoothen the anomalies obtained at the ground surface by projecting the surface mathematically upward above the original datum (Revees, 2005). By implementation of reduction to pole on both the amplitude and phase spectra of the original total magnetic intensity (TMI) grid, the shapes of the magnetic anomalies were simplified so that they appeared like the positive anomalies located directly above the source expected for induce magnetized bodies at the magnetic pole where the angle of inclination is 90° and zero declination.

The derivatives (i.e., first, second vertical derivatives and horizontal derivative) helped to sharpen the edges of anomaly and enhanced shallow features (Revees, 2005). The application of the first vertical derivative in an aeromagnetic data equates to observing the vertical gradient with a magnetic gradiometer in order to sharpen the edges of magnetic anomalies, enhancement of the shallow magnetic sources, suppress the deeper magnetic sources and to give a better resolution of closely-spaced sources computation. Hence, the enhancement processes of Oasis Montaj™ (Geosoft Inc., 2012) in Magmap were used for pre-and post-processing stages. The enhanced data was used to produce total magnetic intensity (TMI) map of the study area, performed vertical derivative of the TMI data to enhance shallow geological features and horizontal derivative to identify geology boundaries in the profile data. Then, the Euler deconvolution module was executed to calculate and determine the spectral depth to buried magnetic rocks within the study area as well as the Source Parameter Imaging (SPI) run to further evaluate the depth. The Centre for Exploration Technology (CET) grid and CET porphyry analyses through textural analyses, lineation detection and vectorization were employed to obtain the lineament and structural complexity analysis of the basin. The CET reveals zones of discontinuity associated with ridges.

Data Processing

Both the qualitative and quantitative approaches were applied to the digitalized aeromagnetic dataset through the following steps: separation of magnetic data, generation of magnetic anomaly maps, and analysis of magnetic anomaly data. Furthermore, the following filtering techniques were applied to remove any possible spurious noise so that attention was placed only on the magnetic anomalies of interest all using the Oasis Montaj software.

Regional- Residual Separation using the Fast Fourier Transform

The Fast Fourier Transform (FFT) was applied to the magnetic data to evaluate the energy spectrum curves and estimate the residual (shallow) and regional (deep) sources. This filter was based on the cut-off frequencies that pass or reject certain frequency values and pass or reject a definite frequency band. The radially averaged power spectrum method was used to determine the depths of intrusive bodies, depths of the basement complex and the subsurface geological structures (Bhattacharyya, 1966).

Edge Detection Methods

The Source Edge Detection (SEDE) function locates edges of geological contacts or peaks from potential field data by analysing the local gradients. The SEDE function estimated the location of abrupt lateral changes in magnetization of upper crustal rocks. The purpose was to identify maxima on a grid of horizontal gradient magnitudes.

Tilt Angle Derivative

Tilt angle derivative (TADR) filter is useful for mapping shallow basement structures and for mineral exploration targets (Miller and Singh, 1994; Verduzco et al., 2004). In magnetic data, the TADR is introduced to enhance structural features or contacts of magnetic sources. TADR is an edge detection filter that is common in potential field methods because it provides insight into the boundaries of the magnetic source especially the potential of intrabasement magnetic intrusions (Miller and Singh,

1994). Positive values are located directly above the sources while negative values are located away from the sources (Ibraheem et al., 2018)

Standard 3D-Euler Deconvolution

The use of 3D Euler Deconvolution (3D-EUD) has become widely spread because it has been automated and rapidly interpreted either as a profile or grid data (Reid *et al.,* 1990, Klingele *et al.,* 1991, Marason and Klingele, 1993, Harris *et al.,* 1996). The 3D-EUD requires three orthogonal gradients (i.e., two horizontal gradients and vertical gradient) of the magnetic data to calculate anomaly source locations (Keating and Pilkington, 2004). This filter was introduced in the potential field methods to estimate the positions of structural lineament in so much that no prior source magnetization direction is required. Accordingly, 3D-EUD requires four sets of grids as input data; the total magnetic field, first horizontal derivative in *x*, *y* and vertical derivative in z-direction. The depth estimated depends on the choice of the corrected structural index (SI) and adequate sampling of data. So, the choice of the SI and used of optimum criteria for selecting solutions are fundamental requirements for successful application of this method. To compute the Euler depth and to produce the Euler depth map, the Standard Euler deconvolution interpretation was carried out in three dimensions by employing Oasis montaj software.

Analytic Signal (Total Gradient)

The analytic signal filter (ASF) is a useful tool in locating the edges and estimation of depth of magnetic bodies because it is formed when the horizontal and vertical gradients of the magnetic anomalies are combined (Roest et al., 1992; Hsu et al., 1996; Ansari and Alamdar, 2009; Aisabokhae *et al.,* 2018). Its formation over a causative body depends on the horizontal coordinate as well as depth and not on the direction of magnetisation (Ndlovu *et al.,* 2015). The success of ASF hinges on its ability to locate and determine depth of magnetic sources relying on a few assumptions made about the nature of the source bodies. For these source bodies, the shape of the amplitude of the analytic signal is a bell-shaped symmetric as it is located directly above the source body. The analytic signal of the total magnetic field is expressed in terms of amplitude, A, and it is estimated from the three orthogonal derivatives of the total magnetic field (*T*). It is defined as the square root of the squared sum of the derivatives in the *x*, *y* and *z* directions of the magnetic field (Roset et al., 1992).

$$|A(x,y,z)| = \sqrt{\left(\frac{\partial T}{\partial x}\right)^2 + \left(\frac{\partial T}{\partial y}\right)^2 + \left(\frac{\partial T}{\partial z}\right)^2} \qquad (1)$$

where $A(x, y, z)$ is the amplitude of the analytic signal at (x, y, z) and T is the observed magnetic field. The $\frac{\partial T}{\partial x}$, $\frac{\partial T}{\partial y}$, $\frac{\partial T}{\partial z}$ are the first derivatives of the total magnetic field.

Source Parameter Imaging

Source Parameter Imaging (SPI) is also known as the local wave number (k). It is a filter used for the estimation of the depths of magnetic sources. The maxima of local wave numbers (k) are situated directly above the isolated contact edges and for a dipping contact, the maxima of the local wave numbers do not depend on magnetic parameters such as the inclination, declination, dip, strike and remnant magnetization (Thurston and Smith, 1997; Saada, 2016). The depth of the magnetic source is estimated as the reciprocal of the local wave number (Eq.3). The Source Parameter Imaging™ (SPI) function of the Oasis Montaj™ extension automatically calculated the depth of magnetic sources from a gridded magnetic dataset. The local wave number (k) was determined from the magnetic field, T as:

$$k = \frac{\frac{\partial^2 T}{\partial x \partial z}\left(\frac{\partial T}{\partial x}\right) - \frac{\partial^2 T \partial T}{\partial x^2 \partial z}}{\left(\frac{\partial T}{\partial x}\right)^2 + \left(\frac{\partial T}{\partial z}\right)^2} \qquad (2)$$

The depth was estimated at the magnetic source edge as the inverse of the local wave number as:

$$\text{Depth}(x = 0) = \frac{1}{k_{max}} \qquad (3)$$

RESULTS AND DISCUSSION

The gridded data referred to as the Total Magnetic field Intensity (TMI) in colour-shaded grid is presented in Figure 4. The map reveals some positive magnetic anomalies (red colour) which appear as circular shape occupying the south to south western parts and associated with negative magnetic anomalies observed in the north and northwestern of the study area. The magnetic intensity ranges from -98.0 nT (minimum) to 222.8 nT (maximum). These variations in magnetic intensities could be linked to degree of strike, variations in depth, volcanic intrusions and changes in lithology or basement topography in the area. Moreso, the positive anomalies are attributed to relatively deep-seated low relief basement structures and volcanic intrusions, suggesting that the TMI anomalies have been strongly influenced by regional tectonics.

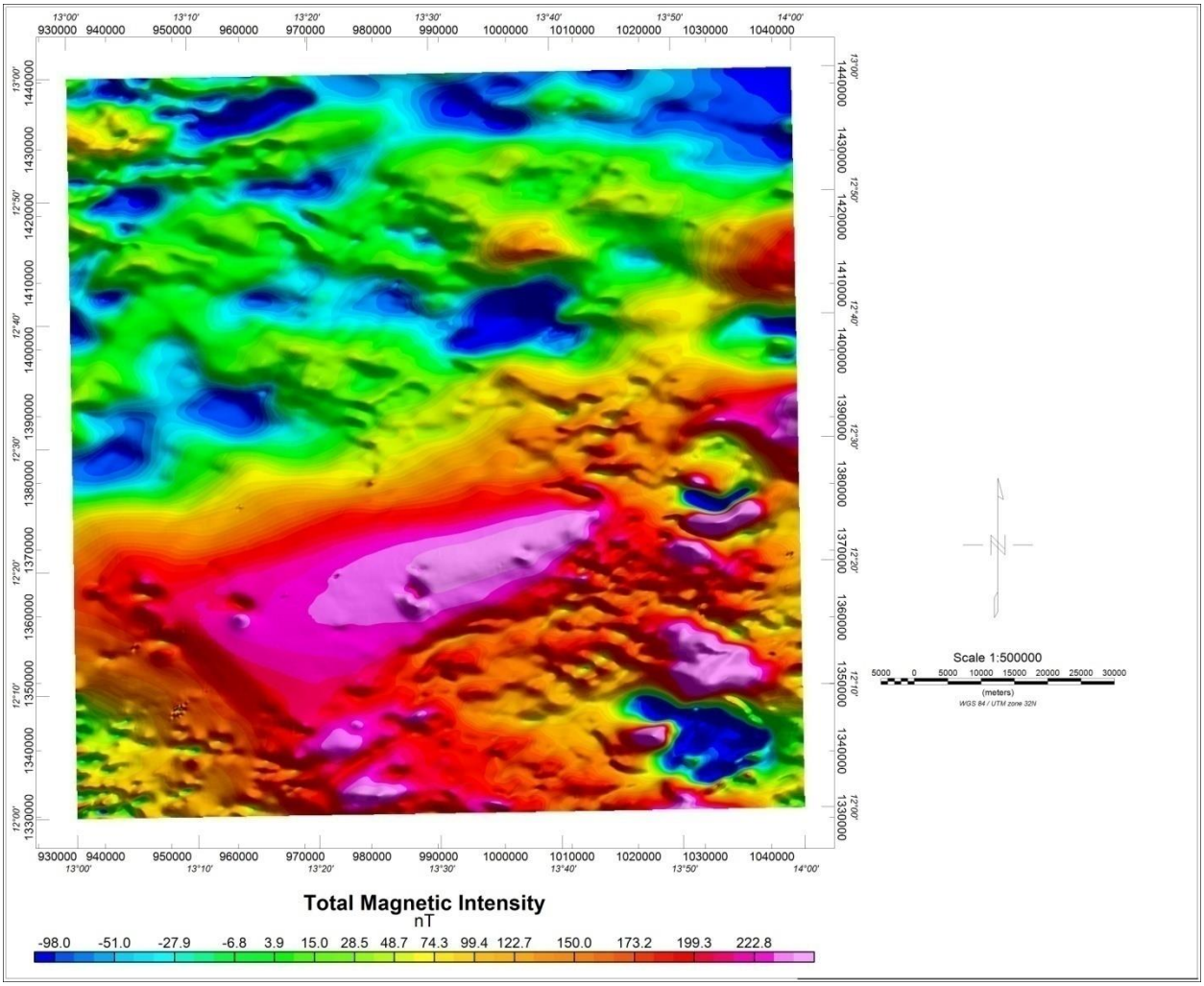

Figure 4: Total Magnetic Intensity Colour-shaded Grid Map of the Entire Study Area

Figure 5 is the lineament map of the study area. The map shows the long regional trends which control the subsurface structure beneath the studied area. The three main dominant structural trends that affect the area are the ENE–WSW, WNW–ESE and E–W. The relationships between these trends suggest that the area has been subject to a number of tectonic events. It is observed that majority of the lineaments identified are located in the northern portion and extends from the east to the west of the area. Figure 6 is a rose diagram used to determine the trend of geological structures in the study area. It shows that the lineaments resulting from the tectonic events such as faults, fractures and dyke intrusions trend in the E-W and EN-WS directions. Figure 7 is a structural complexity map showing the different degrees of deformity or shear zones. It reveals areas of junction high density (red) in the central part believed to be associated with the basement rocks. The map further reveals that there is high lineament density in the NE and SE parts of the area. Also, minor lineaments intersect at the other parts of the area too but very few were identified in the southwestern part. It is believed that the geological structures had occurred probably during the formation of the entire basin.

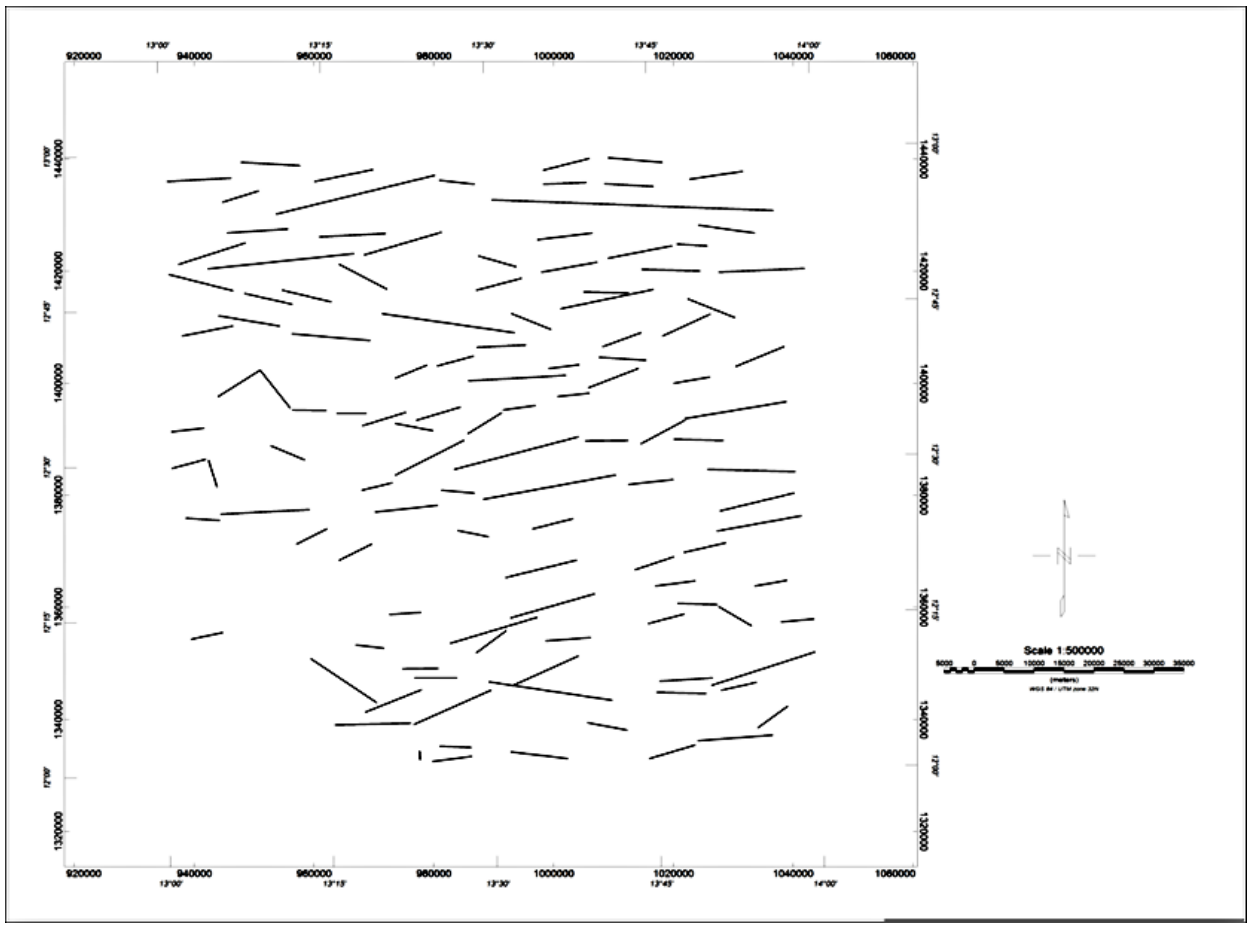

Figure 5: Lineament Map of the Basin

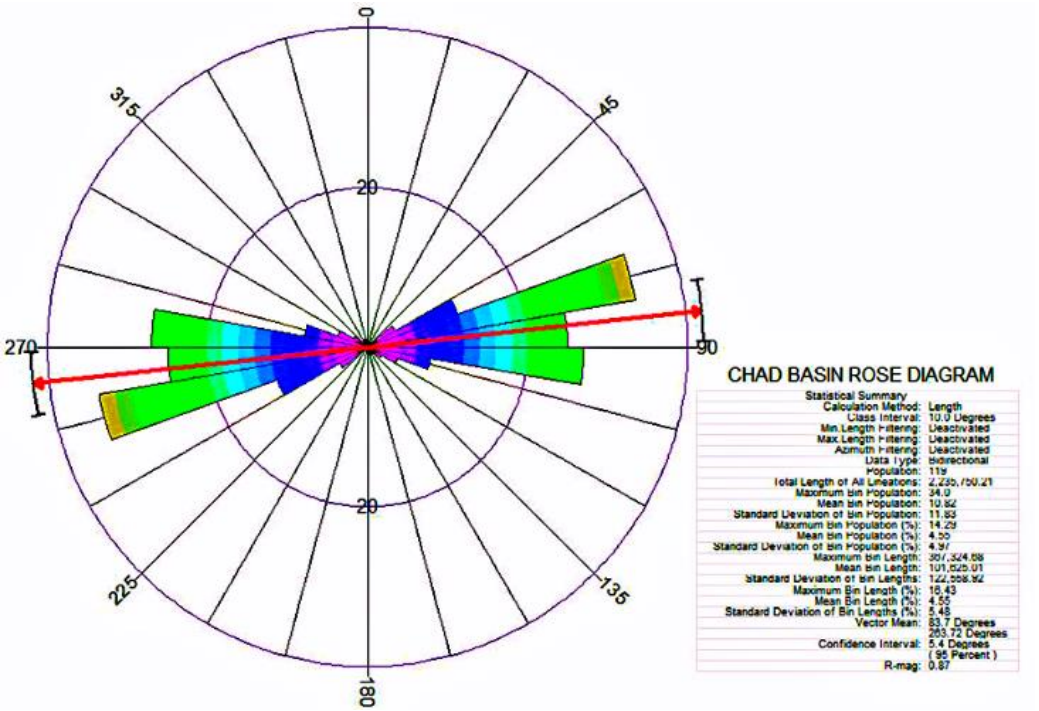

Figure 6: Rose Plot Diagram Showing Major Structural Trend

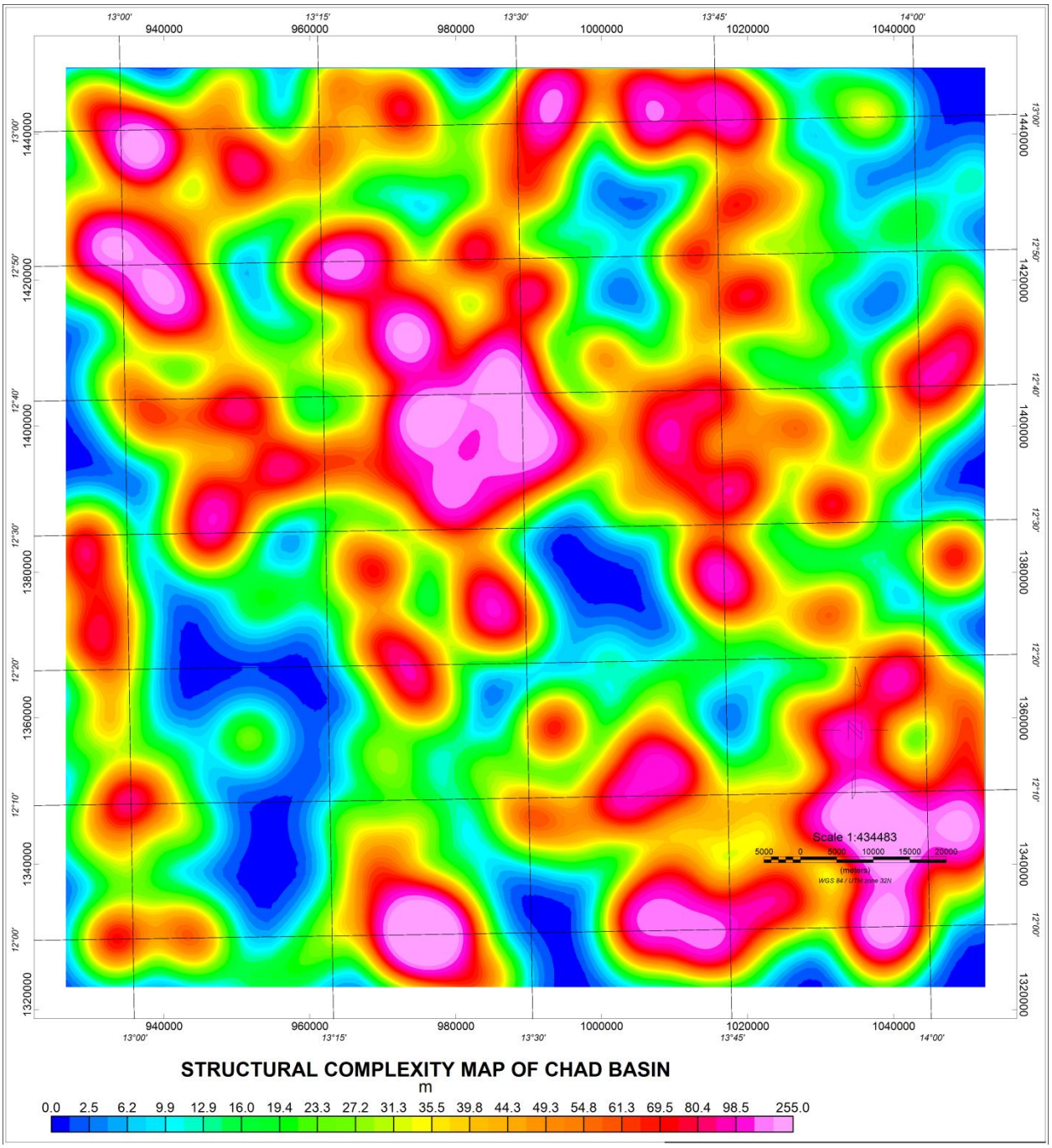

Figure 7: Structural Complexity Map of the Study Area

Figure 8 is the tilt derivative (TDR) map which identifies the shallow basement structures in the area. The TDR enhances geological features and detect the edge of the causative body. It produces a zero value over or close to the source edges and, therefore used to trace the outline of the edges Miller and Singh (1994). Inspection of the tilt derivative map indicated that there was a major source of disturbance which trends in an approximately NE-SW direction. Thus, this large disturbance could be a possible target for future exploration as it has very high magnetic field anomaly.

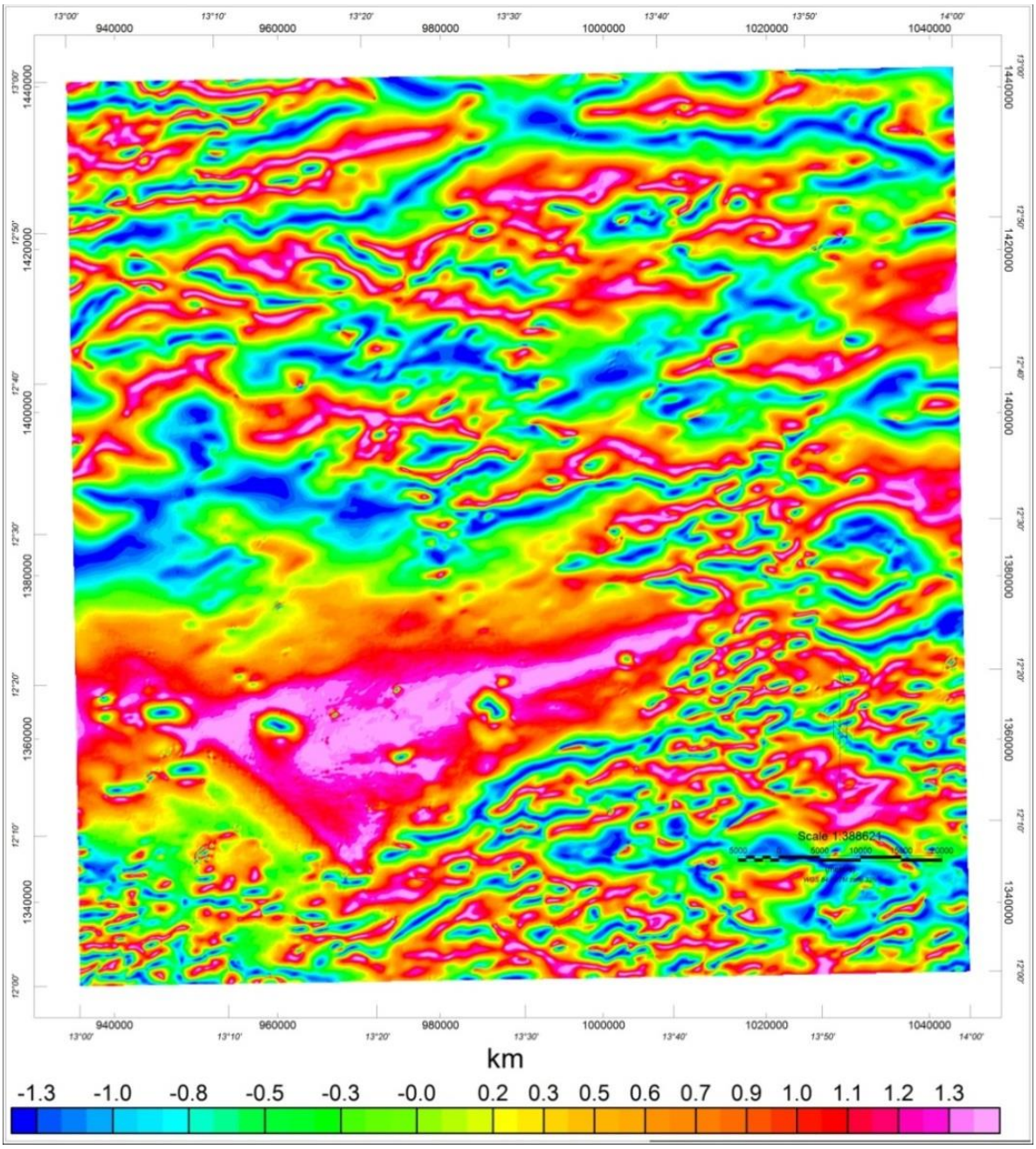

Figure 8: Tilt Derivatives Map of the Study Area

Figure 9 is the 3D Euler Devolution solution map of the study area. In the north-eastern part, the solutions are situated at shallow depth with increasing depth, and in the south-eastern part the solutions are located deeply at depth of about 770 m. In the northwestern part, Euler plots shows non-uniform depth distribution. The maximum depth is greater than 770 m and it is prominent in the southwestern part corresponding to or in consonance with the highest amplitude of the magnetic field intensity. Also, the Euler solution map reveals faults/fractures at depth range of 828 m to 1606 m and dominated the northeastern and northwestern parts of the area.

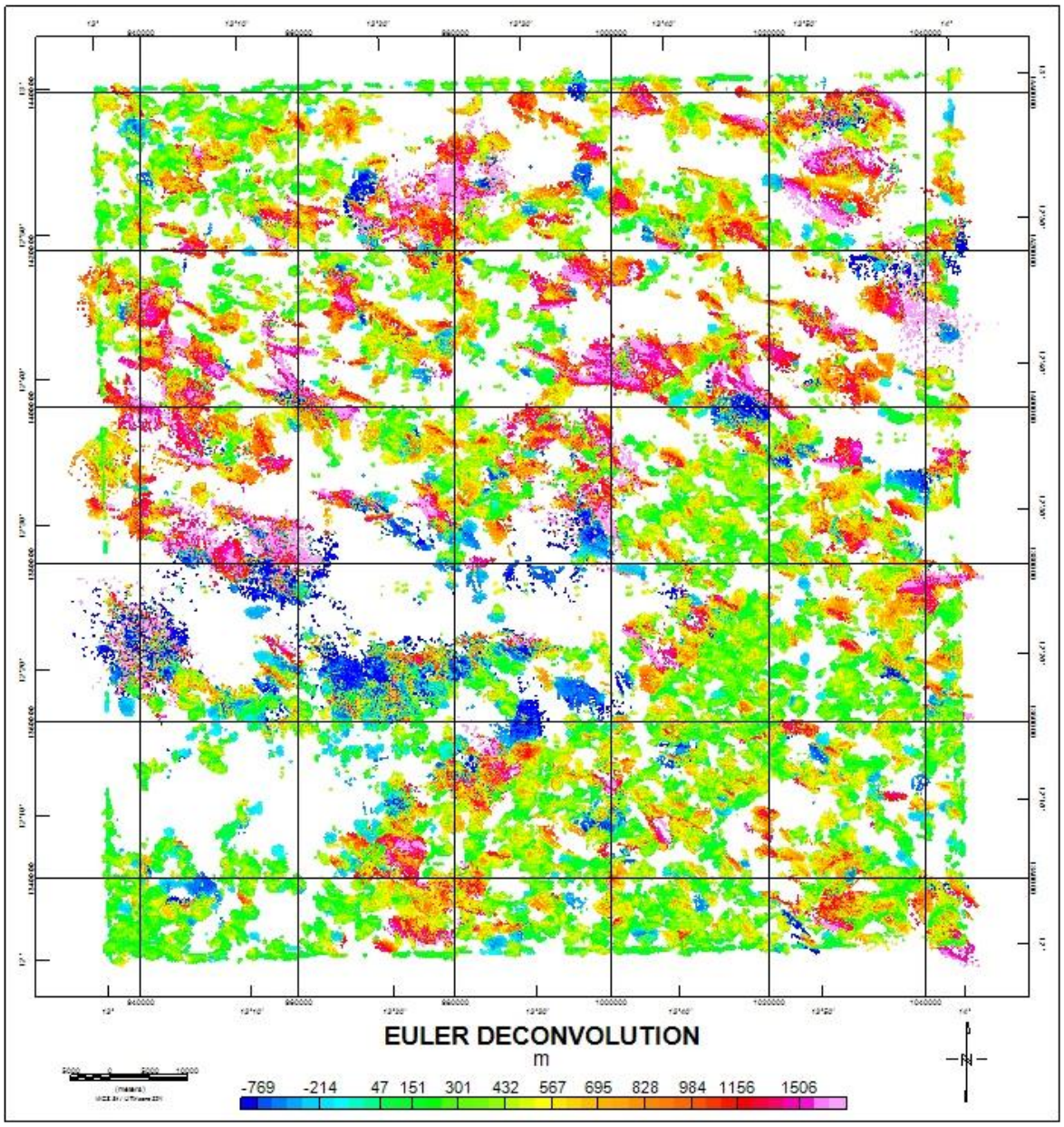

Figure 9: Standard 3D-Euler Deconvolution Plotted on Shaded Color Map of TDR

Figure 10 is the Analytical Signal (AS) relief map of the area estimated from the reduction to pole map using the FFT tool in the frequency domain. Analytical signal is relevant in locating edges of magnetic source bodies and for repositioning the detected magnetic anomalies during interpretation directly over the magnetic sources (Roest et al., 1992). The AS values range from 0.0061nT/m which is visible along the central and western parts to 0.0622 nT/m observed in the south and north-western regions.

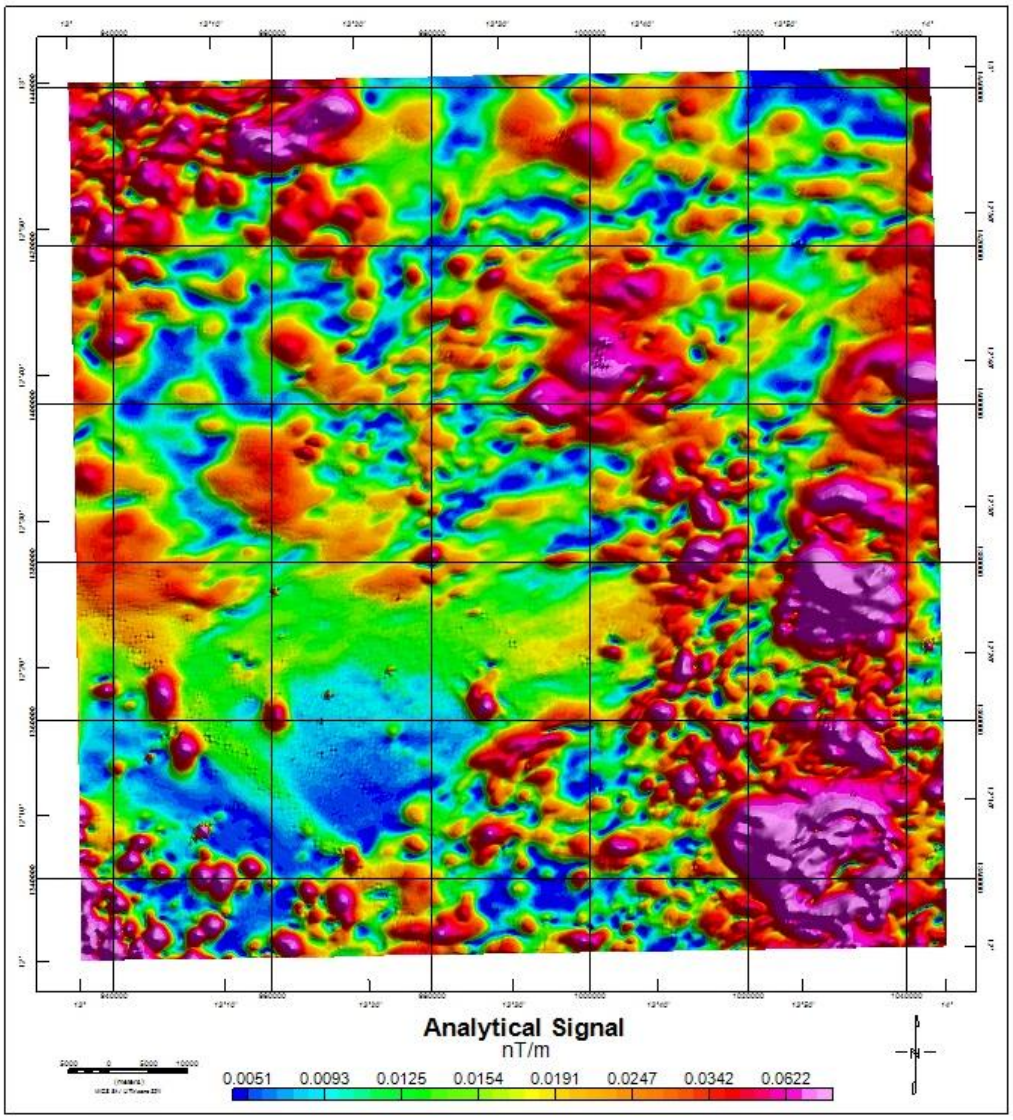

Figure 10: Analytical Signal Colour Shaded Relief Map of the Area Showing Anomaly Texture, Discontinuities in Anomaly Pattern

The radially-average energy power spectrum estimated from the RTP map is shown in Figure 11. From the power spectrum curves, the regional, residual as well as noise signals were determined. The first segment of the plot is in the frequency range of 0.0 to 1.0 cycle/km, represents the regional or deep seated sources with long wavelength. The corresponding depth estimate chart was used to calculate the average depths to the top of the deep and shallow sources. The estimated average depth to the top of regional sources is about 5.4 km while for the shallow sources, the average depth is about 1.5 km.

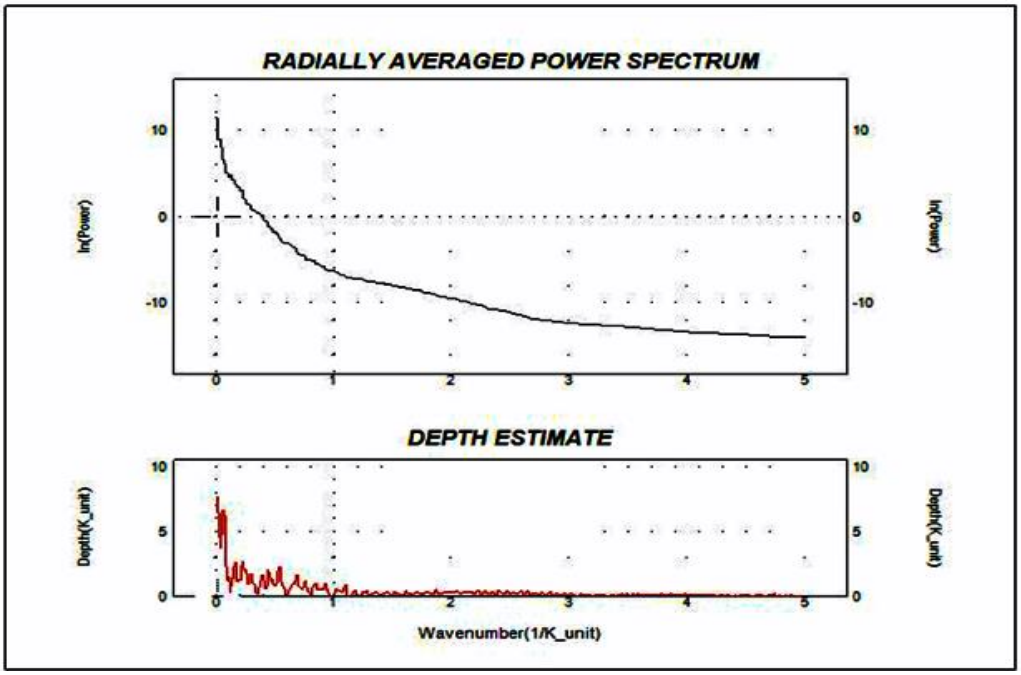

Figure 11: Power Spectrum of Aeromagnetic Data Showing the Corresponding Average Depths

Figure 12 presents the source parameter index (SPI) map of the study area with five representative profiles superimposed across the entire map from which variations in depths are estimated in Figs. 13 (a-e). The negative depth values in the SPI image depict the depths of buried magnetic bodies supposedly the deeply seated basement rocks. The pink colour indicates areas of shallow magnetic bodies the blue colour represents deeply buried magnetic bodies ranging from -3383.8 to -5400.3 m. The SPI depth result ranges from 285.6 m (outcropping and shallow magnetic bodies) to -5400.3 m (deep lying magnetic bodies). The SPI depth map shows great similarity to the depth map produced using analytical signal filter. The depth estimated along profile 1 (i.e. Y^1-Y^1) in Fig.13a has a maximum depth of 8 km with less than 100 nT value on the TMI profile. On profile 2 (Y^2-Y^2), two peaks with depths of about 8 km each with less than -100 nT value are observed (Fig. 13b). Along profile 3 (Y^3-Y^3) in Fig.13c, an average depth greater than 10 km with TMI value of about 0 nT are estimated. In Fig. 13d, several peaks with approximate depth of 10 km and TMI of 240 nT are estimated along profile 4 (Y^4-Y^4). Profile 5 (Y^5-Y^5) has two peaks with estimated depth greater than 16 km and TMI values greater than 0 nT as shown in Fig. 13e.

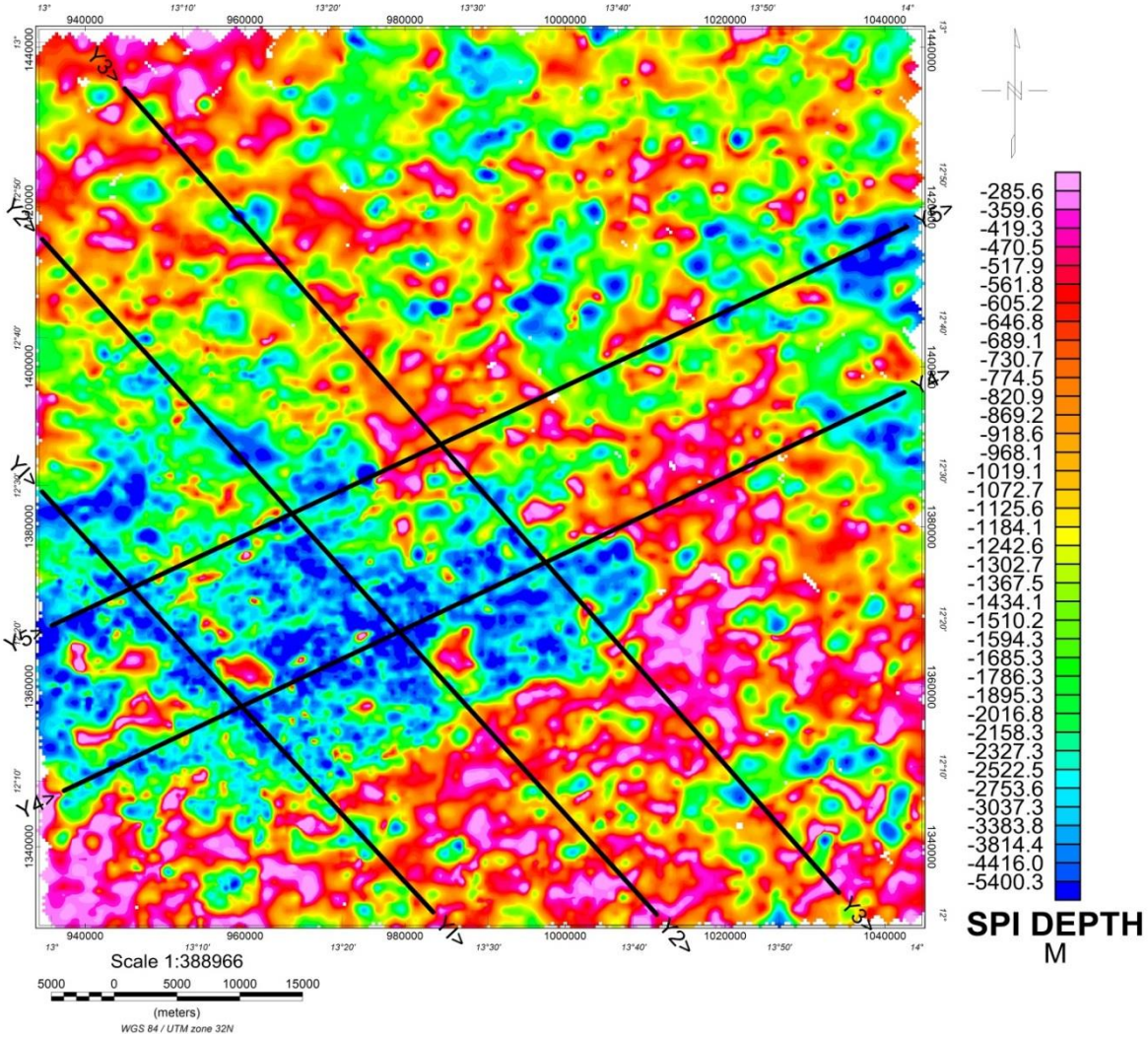

Figure 12: Five Profiles Transacting Across the Source Parameter Imaging (SPI) Map for Depth Estimation of the Study Area

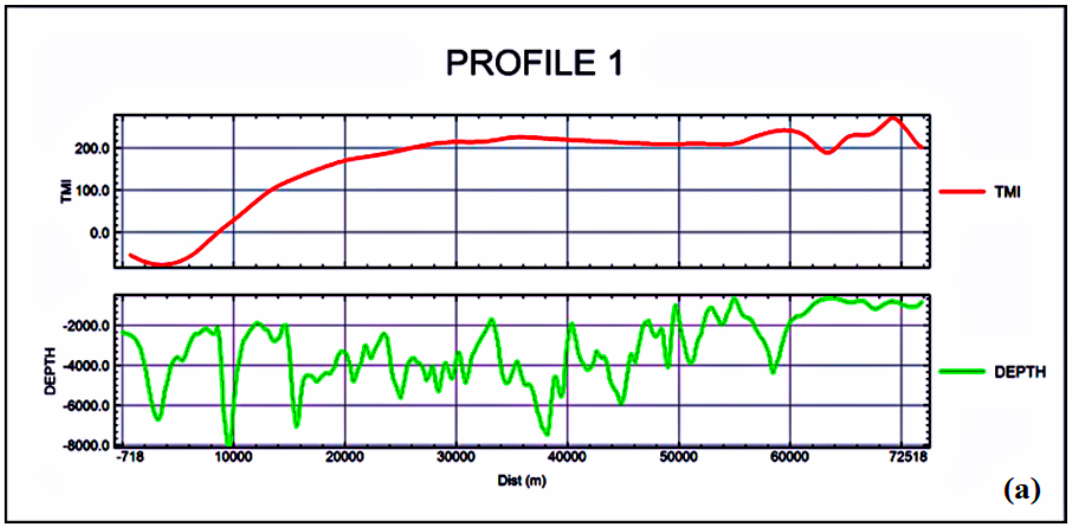

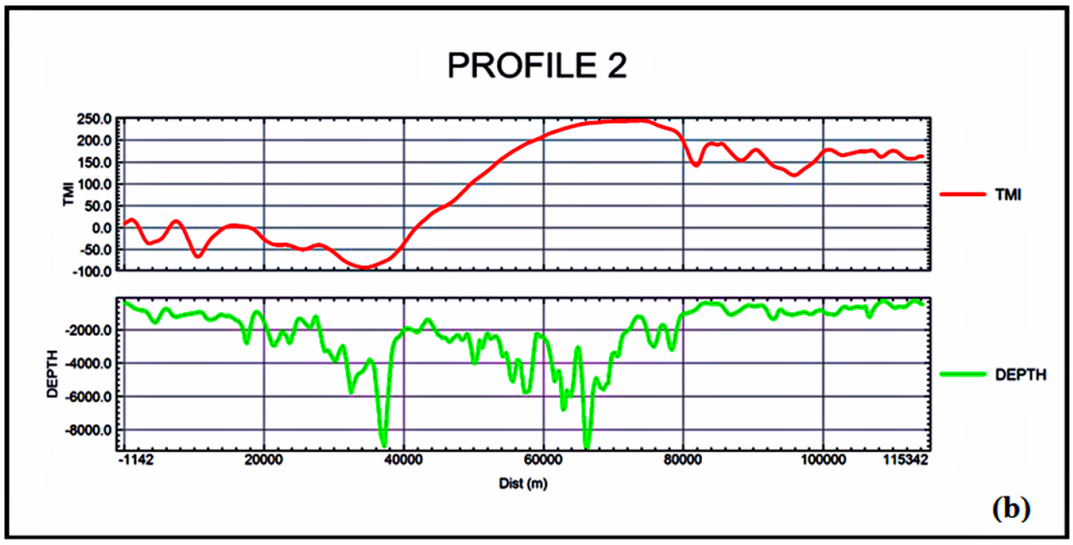
PROFILE 2
TMI
250.0
200.0
150.0
100.0
50.0
0.0
-50.0
-100.0
TMI
DEPTH
-2000.0
-4000.0
-6000.0
-8000.0
DEPTH
-1142
20000
40000
60000
80000
100000
115342
Dist (m)
(b)

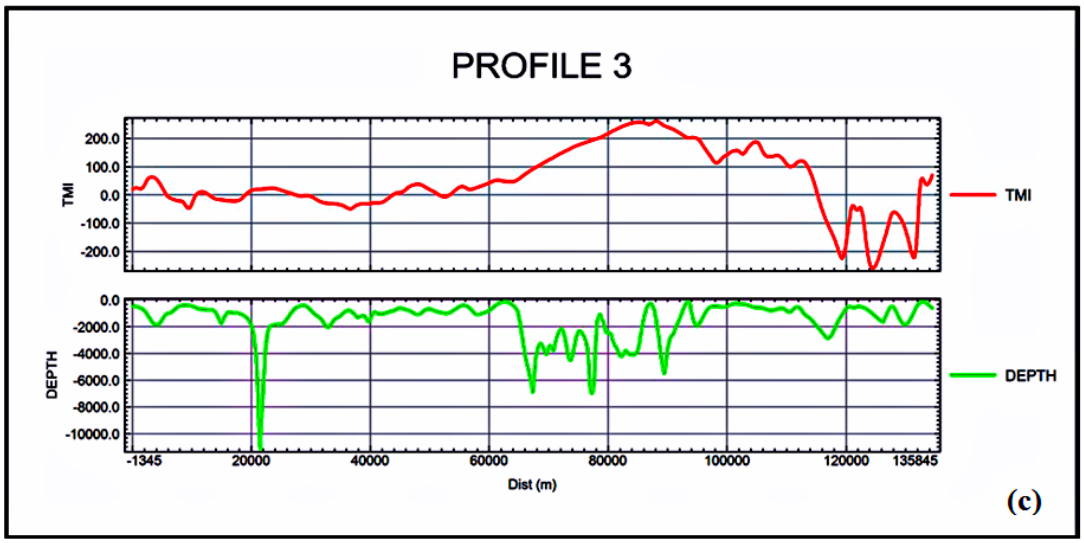
PROFILE 3
TMI
200.0
100.0
0.0
-100.0
-200.0
TMI
DEPTH
0.0
-2000.0
-4000.0
-6000.0
-8000.0
-10000.0
DEPTH
-1345
20000
40000
60000
80000
100000
120000
135845
Dist (m)
(c)

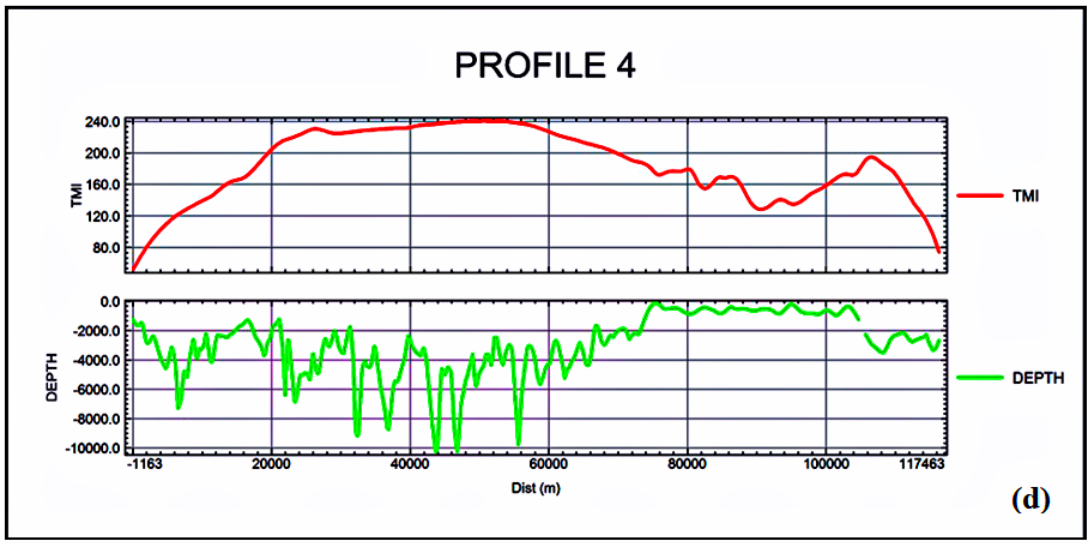
PROFILE 4
TMI
240.0
200.0
160.0
120.0
80.0
TMI
DEPTH
0.0
-2000.0
-4000.0
-6000.0
-8000.0
-10000.0
DEPTH
-1163
20000
40000
60000
80000
100000
117463
Dist (m)
(d)

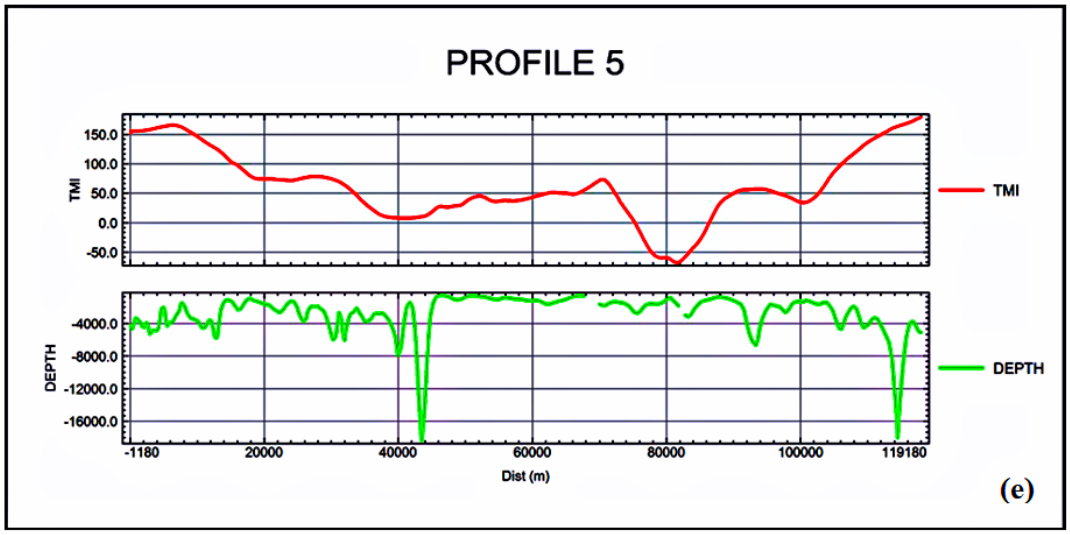

Figures 13: Variations in TMI and Depth Estimation Derived from the SPI Image Across Profiles (a) Y^1-Y^1 (b) Y^2-Y^2 (c) Y^3-Y^3 (d) Y^4-Y^4 (e) Y^5-y^5

CONCLUSION

In this study, the aeromagnetic data sets of the Nigerian parts of the Chad basin have been interpreted, leading to the mapping and detection of some magnetic structures. Morphological differences in the lineament patterns were detected through the CET approach. The existence of lineaments was related to faulting associated with deep-seated basement structures related to the rifting of the continent. The depth to the top of the intrusive causative targets estimated ranges between 256 m to 5.4 km. The depth to the basement of the study area shows clearly that the sedimentary cover deeps towards the western parts and could be significant for favorable hydrocarbon formation than the eastern parts associated with a thin sedimentary cover. The analysis and interpretation of the aeromagnetic data has delineated the lithological and structural setting which may control the deposition of hydrocarbon in the Chad Basin.

ACKNOWLEDGEMENT

The authors gratefully thank the Nigeria Geological Survey Agency for providing Data for the study.

REFERENCES

Aisabokhae, J., Adamu, A., & Oresajo, B. (2018). Analytic signal, depth and multispectral interpretation of areas within the Continental Terminal, North-western Nigeria. *Journal of Applied Sciences and Environmental Management*, *22*(5), 669-673.

Ansari, A.H., & Alamdar, K. (2009) Reduction to the Pole of Magnetic Anomalies Using Analytic Signal. World Applied Sciences Journal, 7, 405-409.

Arogundade, A. B., Hammed, O. S., Awoyemi, M. O., Falade, S. C., Ajama, O. D., Olayode, F. A., & Olabode, A. O. (2020). Analysis of aeromagnetic anomalies of parts of Chad Basin, Nigeria, using high-resolution aeromagnetic data. *Modeling Earth Systems and Environment.* doi: https://doi.org/10.1007/s40808-020-00769-y.

Auken, E. Boesen, T., & Christiansen, A.V. (2017). A review of airborne electromagnetic methods with focus on geotechnical and hydrological applications from 2007 to 2017. Adv. Geophys. 58, 47–93.

Bhattacharyya, B.K. (1966) Continuous Spectrum of the Total Magnetic Field Anomaly Due to a Rectangular Prismatic Body. Geophysics, 31, 197-212. http://dx.doi.org/10.1190/1.1439767.

Biswas, A., & Sharma, S. P. (2020). Advances in Modeling and Interpretation in Near Surface Geophysics. *Springer Geophysics.* https://doi.org/10.1007/978-3-030-28909-6.

Carter, J. D., Barber, W., Tait, E.A and Jones, G.P. (1963). The geology of parts of Adamawa, Bauchi and Borno provinces in north-eastern Nigeria. Bulletin Geological Survey Nigeria. 30, 1-99

Christensen, C.W., Pfaffhuber, A.A., Anschütz, H., & Smaavik, T.F. (2015). Combining airborne electromagnetic and geotechnical data for automated depth to bedrock tracking. Journal of Applied Geophysics, 119, 178-191. https://doi.org/10.1016/j.jappgeo.2015.05.008.

Cox, L.H., Wilson, G.A., & Zhdanov, M.S. (2012). 3D inversion of airborne electromagnetic data. Geophysics, 77, WB59–WB69.

Cratchley, C.R., Louis, P., & Ajakaiye, D.E. (1984). Geophysical and geological evidence for the Benue-Chad Basin Cretaceous rift valley system and its tectonic implications. Journal of African Earth Sciences, 2(2), 141-150.

Djamel, B. (2017) Combining resistivity and aeromagnetic geophysical surveys for groundwater exploration in the Maghnia Plain of Algeria. *J Geol Res.* https://doi.org/10.1155/2017/1309053.

Elliott, P., & Laharia, P. (2008). The Use of Aeromagnetics and Airborne Gravity in Petroleum Exploration. 7th International Conference & Exposition on Petroleum Geophysics. P. 91

Feder, A. M. (1962). Radar geology can aid regional oil exploration. *World Oil,* 155, 130-138. Fischer, W. A. (1964). Geological interpretation from air photos. Proc. Seminar on 19.

Genik, G. J. (1992). Regional framework, structural and petroleum aspects of rift basins in Niger, Chad and the Central African Republic Tectonophysics, vol. 213, 1992, pp. 169-185.

Geosoft Inc. (2012) Oasis Montaj™ v7.2 Software (Standard Edition): Integrated Platform Software for Earth Exploration. Geosoft Inc., Toronto.

Grove, A. T., & Pullan, R. A. (2017). Some aspects of the Pleistocene paleogeography of the Chad Basin. In *African ecology and human evolution* (pp. 230-245).

Hood, P., & Ward, S. H. (1969). Airborne Geophysical Methods. *Advances in Geophysics,* 1–112. https://doi.org/10.1016/s0065-2687(08)60508-7.

Hsu, S. K., Sibuet, J.C., & Shyu, C.T. (1996). High-resolution detection of geologic boundaries from potential anomalies: an enhanced analytic signal technique, Geophysics, 61, 373–386, 1996.

Ibraheem, I.M.; Gurk, M.; Tougiannidis, N.; Tezkan, B. (2018). Subsurface investigation of the Neogene Mygdonian Basin, Greece using magnetic data. Pure Appl. Geophys. 175, 2955–2973.

Innocent, A. J., Chidubem, E. O., & Chibuzor, N. A. (2018). Analysis of aeromagnetic anomalies and structural lineaments for mineral and hydrocarbon exploration in Ikom and its environs southeastern Nigeria. *Journal of African Earth Sciences.* https://doi.org/10.1016/j.jafrearsci.2018.12.011.

Keating, P., & Pilkington, M. (2004). Euler deconvolution of the analytic signal and its application to magnetic interpretation. Geophysical Prospecting 52, 165-182

Kearey, P., Brooks, M., & Hill, I. (2002). An Introduction to Geophysical Exploration. Blackwell Science Ltd., Oxford.

Kivior, I., & Boyd, D. (1998) Interpretation of the aeromagnetic experimental survey in Eromanga/Cooper Basin. *Can J Explor Geophys*, 34:58–66.

Klingele, E., Marson, E.I., & Kahle, H.G. (1991). Automatic interpretation of gravity gradiometric data in two dimensions: vertical gradient, Geophysical Prospecting, 39, 407–434.

Lattman. L. H. (1963). Geologic interpretation of airborne infrared imagery, Photo. 26. Levine, D. (1960). "Radar grammetry," p. 330. McGraw-Hill, New York.

Liang, S., Sun, S., & Lu, H. (2021). Application of Airborne Electromagnetics and Magnetics for Mineral Exploration in the Baishiquan–Hongliujing Area, Northwest China. *Remote Sensing, 13(5), 903.* https://doi.org/10.3390/rs13050903.

Marson, I., & Klingele, E. E. (1993). Advantages of using the vertical gradient of gravity for 3-D interpretation, Geophysics, 58(11), 1588–1595.

Meng, Q., Hu, H., & Yu, Q. (2006). The application of an airborne electromagnetic system in groundwater resource and salinization studies in Jilin, China. J. Environ. Eng. Geophys. 11, 103–109.

Miller, H.G., & Singh, V. (1994) Potential Field Tilt a New Concept for Location of Potential Field Sources. Journal of Applied Geophysics, 32, 213-217. https://doi.org/10.1016/0926-9851(94)90022-1.

Nabighian, M. N. (1972). The analytic signal of two-dimensional magnetic bodies with polygonal cross-section: its properties and use for automated anomaly interpretation, Geophysics, 37(3), 507–517.

Nabighian, M. N. (1974). Additional comments on the analytic signal of two-dimensional magnetic bodies with polygonal cross-section, Geophysics, 39(1), 85–92.

Nabighian, M. N. (1984). Toward a three-dimensional automatic interpretation of potential field data via

generalized Hilbert transforms: Fundamental relations, Geophysics, 49(6), 780–786.

Ndlovu, T., Mashingaitze, R. T., & Mpofu, P. (2015). Analytic signal and Euler depth interpretation of magnetic anomalies: applicability to the Beatrice Greenstone Belt. *Journal of Geography and Geology*, *7*(4), 108-112.

Noh, K., Yoon, D., & Byun, J. (2020). Imaging subsurface resistivity structure from airborne electromagnetic induction data using deep neural network. *Explor. Geophys*., 51, 214–220.

Obaje, N.G. (2009). The Bornu Basin – Nigerian Sector of the Chad Basin. Geology and Mineral of Nigeria, 120, 69 – 76.

Obaje, N. G., Umar, U. M., Aweda, A. K., & Ozoji, T. M. (2020). Nigerian Cretaceous coal deposits and their petroleum source rock characteristics. *International Journal of Petroleum and Gas Exploration Management*, *4*(1), 1-14.

Ogah, A.J., & Abubakar, F. (2024). Solid mineral potential evaluation using integrated aeromagnetic and aeroradiometric datasets. *Sci Rep* 14, 1637 (2024). https://doi.org/10.1038/s41598-024-52270-6

Okpoli, C.C., & Akinbulejo, B.O. (2022). Aeromagnetic and electrical resistivity mapping for groundwater development around Ilesha schist belt, southwestern Nigeria. *J Petrol Explor Prod Technol* 12, 555–575. https://doi.org/10.1007/s13202-021-01307-x.

Palacky, G. J. (1981). The airborne electromagnetic method as a tool of geological mapping. Geophysical Prospecting, 29(1), 60–88. https://doi.org/10.1111/j.1365-2478.1981.tb01011.x.

Petters, S.W., Ekweozor, C.M. (1982) Petroleum geology of Benue Trough and southern Chad Basin Nigeria. AAPG Bull 66:1141–1149

Rajaram, M., Anand, S. P., Hemant, K., & Purucker, M. E. (2009). Curie isotherm map of Indian subcontinent from satellite and aeromagnetic data. *Earth and Planetary Science Letters*, *281*(3-4), 147-158.

Rambabu, H.V., & Sinha, G.D.J. (1986) Magnetic anomalies over thin plates and their analysis. *Earth Planet Sci* 95(3):331–341.

Reford, M. S., & Butt, G. R. (1983). Aeromagnetics in Australian petroleum exploration. *Exploration Geophysics*, 14(4), 113. https://doi.org/10.1071/eg983113.

Reeves, C. (2005). Aeromagnetic Surveys: Principles, practice and interpretation. Geosoft, Earth- works, Washington DC, 155 p.

Reid, A. B., Allsop, J. M., & Granser, H. et al. (1990). Magnetic Interpretation in Three Dimensions Using Euler Deconvolution. Geophysics, 55, 80-91. https://doi.org/10.1190/1.1442774

Roest, W.R., Verhoef, J., & Pilkington, M. (1992) Magnetic Interpretation Using 3-D Analytic Signal. Geophysics, 57, 116-125. http://doi.org/10.1190/1.1443174

Rydstrom, H. 0. (1967). Interpreting local geology from radar imagery, *Geol. Soc. Am. Bull*., 78, 429-436.

Saada, S. A. (2016). Edge detection and depth estimation of Galala El Bahariya Plateau, Eastern Desert-Egypt, from aeromagnetic data. Geomechanics and Geophysics for Geo-Energy and Geo-Resources, 2, 25-41.

Sharma, P.V. (2002). Geophysical Methods in Geology, Elsevier Scientific Publishing Company, Amsterdam, The Netherlands, 1976, pp. 1–211.

Smith, R.S., O'Connell, M.D., & Poulsen, L.H. (2004). Using airborne electromagnetics surveys to investigate the hydrogeology of an area near Nyborg, Denmark. Near Surf. Geophys. 2, 123–130. https://doi.org/10.3997/1873-0604.2004009

Srivastava, S., & Agarwal, B. N. P. (2010). Inversion of the amplitude of the two-dimensional analytic signal of the magnetic anomaly by the particle swarm optimization technique. *Geophysical Journal International*, *182*(2), 652-662.

Styles, P. (2012). *Environmental Geophysics: Everything you ever wanted (needed!) to know but were afraid to ask!* EAGE.

Thurston, J.B., & Smith, R.S. (1997). Automatic Conversion of Magnetic Data to Depth, Dip, and Susceptibility Contrast Using the SPITM Method. *Geophysics*, 62, 807-813. https://doi.org/10.1190/1.1444190.

Verduzco, B., Fairhead, J.D., Green, C.M., & MacKenzie, C. (2004) New Insights into Magnetic Derivatives for Structural Mapping. The Leading Edge, 23, 116-119. https://doi.org/10.1190/1.1651454.